Indian Journal of Chemistry
Vol. 64, January 2025, pp. 85-92
DOI: 10.56042/ijc.v64i1.14909

Structural and optical properties of manganese-doped cobalt thin films prepared by spray pyrolysis

Amol S Mandle*[a], Aishwarya V Kamble[a] & M A Barote[b]

[a] Department of Physics, Dayanand Science College Latur 413 512, Maharashtra, India

[b] Department of Physics, Azad Mahavidyalaya, Ausa, Dist. Latur 413 520, Maharashtra, India

E-mail: asmandle@gmail.com, barotema1971@gmail.com

Received 7 November 2024; accepted (revised) 27 December 2024

This paper presents the deposition of manganese-doped cobalt ferrite (CoMnF) thin films on FTO substrates using spray pyrolysis. Optimization of the crucial growth parameters, along with annealing at 450°C for 2 hours, has led to a single-phase cubic spinel structure without any extraneous peaks confirmed by X-ray diffraction. The films have interplanar distances between 4.896 to 1.484 Å, crystallite sizes are small: FWHM: 0.338° to 0.497°, and the lattice constant is 8.418 Å. FTIR has identified a peak at 431 cm^{-1}, with implications for the presence of the ferrite phase due to the existence of octahedral metal-oxygen stretching. The UV-Vis spectra reveal strong absorption at 215 nm and 347 nm. The direct bandgap has been found to be 5.6 eV. Raman vibrational modes are affected due to Mn doping. These Mn-doped Co-ferrite thin films have properties that are well suited for application in supercapacitors, sensors, and energy storage devices.

Keywords: Thin film, Spray pyrolysis, Cobalt ferrite, Structural properties

Ferrites have gained prominence over pure metals as magnetic materials due to their cost-effectiveness, high resistivity, robust magnetic properties, and improved mechanical strength[1]. These advantages make ferrites particularly valuable in both technological and industrial applications. Among magnetic materials, ferrites play a crucial role, especially in thin film form, where they are efficient nanostructures with versatile applications, demonstrating higher performance compared to other nanomaterials. Significant research has focused on enhancing the magnetic and electrical properties of spinel ferrite thin films by substituting divalent and trivalent metal ions, making them suitable for use in memory storage devices, transformer cores, and high-frequency devices[2,3]. Cobalt ferrites are especially notable for their affordability and valuable magnetic and electrical properties, which enable their use in devices such as microwave devices, isolators, circulators, and phase shifters. This is largely due to their unique rectangular hysteresis loop characteristics, which are essential for such applications. The intrinsic properties of ferrites are influenced by several factors, including their chemical composition, synthesis methods, heat treatment, and ion substitution[4]. It is well-established that parameters like the purity of raw materials, preparation techniques, annealing temperatures, dopant concentrations, and impurities significantly impact the supercapacitive and electronic properties of ferrites[5]. As a result, many studies have explored how various additives affect the electromagnetic characteristics of ferrites. However, research on Mn^{2+} -substituted cobalt ferrite thin films remains limited[6]. A few notable studies provide insight into the effects of manganese substitution on cobalt ferrites. J. Dash and colleagues investigated the magnetic properties and crystallization of sputter-deposited Co-Mn ferrite thin films. Their findings revealed that the as-deposited films were amorphous, as determined by X-ray diffraction, yet showed promising magnetic properties and high-field susceptibility. Post-annealing between 500°C and 850°C led to crystallization and increased saturation magnetization, a change attributed to adjustments in grain size, intrinsic stress, cation distribution, and crystallinity. In another study, V. Rathod *et al.* synthesized and examined Co-Mn ferrite powders using the combustion technique[7]. They observed that higher Mn^{2+} content reduced saturation magnetization, but the combustion process itself was deemed cost-effective. Additionally, Mahmoud Mahmoudi *et al.* studied the influence of sintering temperature on the magneto-dielectric properties of $Li_{0.30}Mn_{0.4}Fe_{2.30}O_4$ (Ref. 8). They concluded that both density and grain growth were sensitive to sintering temperature and nano-SiO_2 content, with SiO_2 content above 2 wt% decreasing

grain size, while lower SiO_2 concentrations promoted greater density and grain growth. Various methods are available for synthesizing ferrite thin films, including pulsed laser deposition, atomic layer deposition, sol-gel techniques, RF sputtering, spin coating, bath deposition, and spray pyrolysis[9]. Of these, spray pyrolysis has gained traction due to its unique advantages in thin film production. This technique is relatively simple and versatile, enabling the deposition of films over large areas with minimal equipment. By adjusting the solution composition, spray pyrolysis can be adapted to different materials, allowing for multicomponent film deposition. Additionally, it is highly cost-effective, requiring low energy input and eliminating the need for high-vacuum conditions, which reduces operational costs[10]. A key benefit of spray pyrolysis is the precise control it offers over film thickness and morphology by adjusting variables such as spray rate, substrate temperature, solution concentration, carrier gas, and droplet size. This control makes spray pyrolysis highly scalable, which is essential for industrial applications requiring large-scale film production, particularly in fields like solar cells, sensors, and energy storage devices[11]. The technique also supports layer-by-layer deposition, allowing for films with specific thicknesses or multilayered structures. Its adaptability is another major advantage, as it can deposit films on substrates with complex shapes, providing versatility for a wide range of applications[12]. Due to these benefits, spray pyrolysis is extensively used in producing thin films for various applications, including solar cells, sensors, supercapacitors, and solid oxide fuel cells[13]. In this study, we specifically investigate the structural properties and supercapacitive potential of Mn^{2+} -substituted cobalt ferrite thin films, which exhibit promising electrical characteristics and stability. These enhanced properties make Mn-doped Co-ferrite thin films strong candidates for energy storage applications, particularly in supercapacitors. By optimizing key growth parameters, we aim to demonstrate the feasibility of using these films in high-performance energy storage devices.

Experimental Section

Materials used

Raw material ferric nitrate [$Fe(NO_3)_3.9H_2O$] of $Mn(NO_3)_2•4H_2O$ (Mn^{+2}, 71 g/mol) and Co $(NO_3)_2.6H_2O$, Cobalt nitrate was supplied of AR grade (Merck) which was directly applied to prepare the experiment with no additional purification procedure required and metal nitrates of citric acid at the ratio 1:3 was adopted to acquire reaction condition properly. Stabilization was done and adjusted to *p*H 8 by using ammonia solution NH□OH for important aspects regarding the achievement of the thin film's desired composition and properties. All were used during the process-cotton, chromic acid, acetone, and FTO substrates plus distilled water.

Deposition of Thin Film

Thin films with the chemical formula $Co_{0.6}Mn_{0.4}Fe_2O_4$ of Mn^{2+} -substituted cobalt ferrite were deposited using the spray pyrolysis deposition (SPD) technique on FTO substrates. The metal nitrates were dissolved in individual stoichiometric amounts of distilled water. The preparation of the deposition solution involved the mixing of cobalt nitrate, manganese nitrate, and ferric nitrate solutions in a molar ratio of Me^{2+}/Fe^{3+}, where Me^{2+} = $Co_{0.6}$+ $Mn_{0.4}$. This solution was deposited onto a preheated FTO substrate. During the whole process, optimal deposition parameters were used (Table 1). After deposition, the annealing process was carried out at 450°C for 2 h and was cooled down to RT in an air atmosphere. The setup for the thin film preparation *via* spray pyrolysis is illustrated in Fig. 1.

Characterization techniques

X-ray diffraction with an X'pertPro MPD PANalytical system was used to examine the Co films structure. All the measurements were carried out over

Table 1 — Optimized parameters for Mn-doped Co-ferrite thin film deposition for x = 0.4

Parameter	Description
Solution Concentration	1:4 M
Volumetric ratio	1:1
Deposition temperature	360°C
Annealing temperature	450°C for 2 h
Distance between substrate to nozzle	25 cm
Spray rate	1.5 mL /min
Air pressure	0.2 MPa

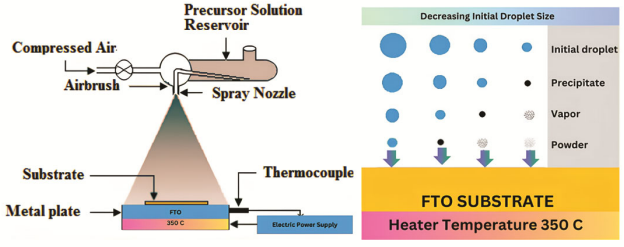

Fig. 1 — Setup for preparation of thin film by spray pyrolysis

Table 2 — Miller indices of the Mn-doped Co-ferrite thin film for x = 0.4

h	k	l	2θ	θ	Sinθ	2Sinθ	d	(a/d)^2	a
1	1	1	18.1	9.050	0.157	0.315	4.896	2.930	8.480
2	2	0	30	15.000	0.259	0.518	2.975	7.932	8.416
3	1	1	35.36	17.680	0.304	0.607	2.536	10.921	8.410
4	0	0	42.98	21.490	0.366	0.733	2.102	15.891	8.409
5	1	1	56.94	28.470	0.477	0.954	1.616	26.907	8.394
4	4	0	62.5	31.250	0.519	1.038	1.484	31.867	8.398
									8.418

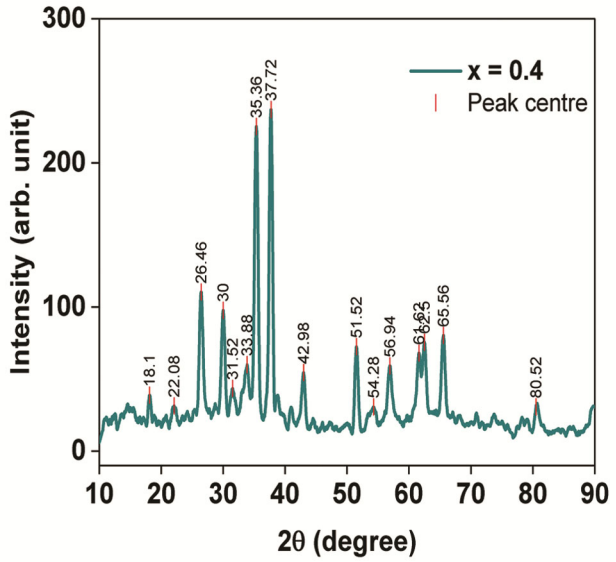

Fig. 2 — X-ray diffraction pattern of Mn-doped Co-ferrite thin film for x = 0.4

the 2θ range of 20° to 80° and with Cu Kα radiation at RT, whose wavelength was set to λ = 1.5405 Å. The surface topography of the CoMnFe-oxide thin film was studied with a PARK Model-XE 7 atomic force microscope in Head mode. SEM analysis was carried out with FEG-Scanning Electron Microscope, Model JSM-7600F, at the SAIF at IIT Bombay, Mumbai. The measurement parameters were adjusted to be accurate with the probe: 17.69 nm amplitude and frequency of 309.68 kHz, and the scanning rate was set at 0.5 Hz.

Results and Discussion

X-ray diffraction analysis

Fig. 2 shows the XRD pattern of Manganese doped Cobalt ferrite thin film. The XRD result manifested peaks at definite values of 2θ corresponding to the Miller indices of cubic spinel structure, reflecting the presence of the spinel phase in all composition. Besides that, defined peaks are witnessed at (111), (220), (311), (400), (511), (440), and (622) toward expressing the similar cubic spinel structure[14]. The manganese ion incorporation into the film matrix, which substitutes cobalt ions, results in an increase in the factors determining the lattice parameters, and a progressive shift toward higher angles of diffraction. The latter is consistent with the expected changes in the lattice caused by the difference in the ionic radii between manganese and cobalt ions[9]. Changes in the peak intensity and broadening with variation of composition are indicative of a possible difference in the crystallinity of the such thin films and some degree of stress or particle size variation. In many of the XRD patterns although all the film samples indicated spinel structure in all the films, the same spinel structure in turn was affected by the manganese content in the films along with the lattice parameters as well as the micro structural features[15].

In Table 2, the Miller indices of the Mn doped Co ferrite thin film for (x = 0.4) are shown, which reveal some information into the crystallographic features. The indices (h, k, l) are lacking in definition, regarding elongate inter planar sections within the crescent cubic spinel phase, assuring the evolution of crystalline phase in the thin film. Values for angle 2θ the angles which correspond to these dip values will fill the peaks with diffracted peaks this will be very informative as structural details of the crystals come to light. the distances about d inter planer from 4.896 and 1.484 reflect the inter-cationic distances decreasing when it takes an increase in values such is always the case concerning material materials especially the crystalline varieties[16]. The increasing values of sin theta's correlation enable the wise to determine this lattice parameter. Since ionic radius of manganese being lower than cobalt, hence manganese ions get incorporated in the progressive manner. An average lattice constant inferred the lattice constant of 8.418Å confirms that its crystalline structure is of a moderate progression. The results also validate the stability of the Mg doped Co ferrite thin films with Mn additives using the sol gel spin coating method[17].

Table 3 — FWHM, Crystallite size (D), dislocation density (δ), lattice strain (ε), of the Mn-doped Co-ferrite thin film for x = 0.4

2θ	θ in Degree	Radian(θ)	FWHM Degree (θ)	FWHM Radian (θ)	Cos θ	D= 0.9λ/βCosθ	D nm	$\delta*10^3$ (nm^{-2})	$\varepsilon*10^{-3}$
18.1	9.05	0.158	0.338	0.006	0.988	238.121	23.812	1.763	0.234
30	15	0.262	0.481	0.008	0.966	170.864	17.086	3.425	0.563
35.36	17.68	0.308	0.551	0.010	0.953	151.174	15.117	4.375	0.767
42.98	21.49	0.375	0.692	0.012	0.931	123.420	12.342	6.564	1.189
56.94	28.47	0.497	0.656	0.011	0.879	137.684	13.768	5.275	1.553
62.5	31.25	0.545	0.356	0.006	0.855	260.943	26.094	1.468	0.943
							18.037		

Table 3 shows useful data in the calculation of FWHM, D, δ and ε are carried out to be used for Mn doped Co-ferrite thin film with x = 0.4. The FWHM values in the range of (0.338° - 0.497°), indicate the existence of peaks with wider peaks in XRD patterns, and consequently, confirm on small size of crystalline and highly strained lattices. This trend is supported even by the crystallite size (D), that show a decrease from (238.121) at the angle of (18.1°) to (123.420) at (42.98°). This means that more and smaller crystallites are formed with highly strained lattices. The dislocation density was defined, δ: $\delta = (23.812\times10^{-3} - 26.094\times10^{-3})$ nm² increased and this indicates an increased degree of defects within the interior of the crystal; an increased dislocation is normally a characteristic which usually goes on to influence a large extent the magnetic or the electrical properties of the concerned material. Further importantly, lattice strain values were ranging from $(0.234\times10^{-3} - 1.189\times10^{-3})$ were consistent with the shrinkage of the crystallite size and the increase in the dislocation density.

Microstructure of CoMnFe-oxide thin film

The SEM image of the Mn-doped Co-ferrite thin film with (x = 0.4), as shown in Fig. 3, helps to explain some of the morphologies. The thin film carries the form of cells in a cluster and agglomerated nature, with the spherical and rough shapes being predominant. This clustering also implies a certain degree of agglomeration, which could be dependent on surface energy effects and magnetic interactions of the particles. Further, the size distribution of the thin film is relatively wide, implying the presence of bigger aggregates as well as smaller nanoparticles within the thin film. This type of size distribution of the particles probably indicates perhaps that no total control is applied in the synthesis so that uniform growth of the nanoparticles was not achieved in the synthesis. The thin film also has very interesting rough and rather uneven surfaces, which should be appreciated for they signify some level of porosity and hence a larger surface area would be created for reaction to occur. Such enhanced surface area would be very useful in the case of drug and or catalysis applications where more interaction with the surrounding is needed. In conclusion, the SEM examination contributes to the knowledge of the structure and possible functionality of the Mn-doped Co-ferrite thin film, pointing out its structural attributes and possible functionality towards the practical[18].

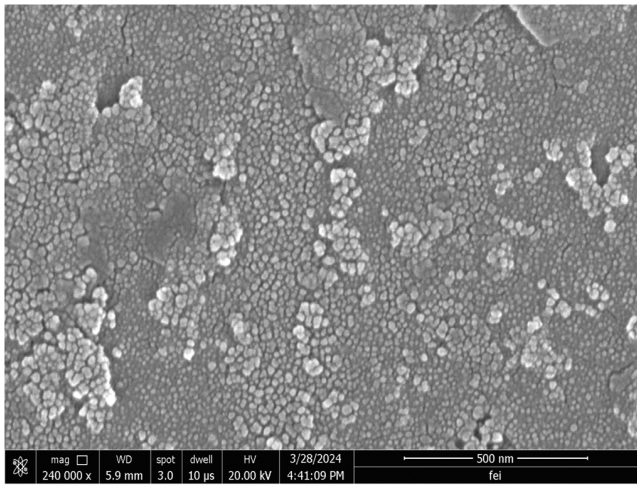

Fig. 3 — SEM image of Mn-doped Co-ferrite thin film x = 0.4

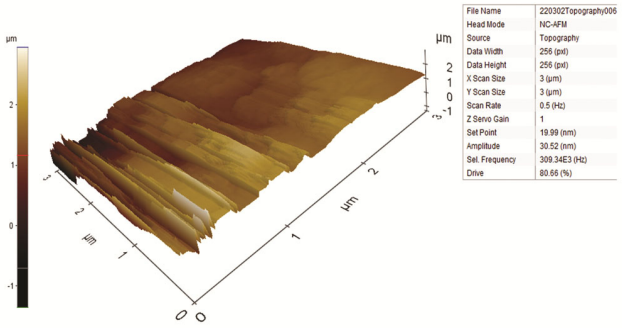

Fig. 4 — AFM image of Mn-doped Co-ferrite thin film x = 0.4

Topography of Mn-doped Co-ferrite thin film

Fig. 4 shows the obtained AFM images. Hooke's law dictates the operation of the AFM, whereby the

force applied to an object is proportional to its displacement. At the atomic scale, the AFM interacts with the surface through van der Waals forces, which are attributed to electromagnetic interactions between atoms and molecules. During the scanning process, the strong reflected laser beam was used to image the integrated film surface morphology characteristics by evaluating the features in terms of roughness or smoothness with a characteristic texture that should occur on the same side. Data showed inhomogeneous topology of a given surface and consequently assumed several material morphology variation across them. This analysis shows a tendency for cluster formation of nanorods or agglomeration of nanoparticles with possible changes in any relevant function property. It is only through a comprehensive characterization of these surfaces that understanding surface characteristics to a larger extent will also determine whether significant impacts toward the various performance criteria observed in its potential applications--such as catalysis, drug delivery, and even energy storage. AFM analysis helps extract critical micro-structural information that establishes foundations for deeper probes into other potential technologies within the horizon of its prospective applications from technology to material science[19].

FTIR spectra of Mn-doped Co-ferrite thin film

From the FTIR spectrum of Fig. 5, some vibrational modes are established for the Mn-doped Co-ferrite thin film with x = 0.4. As can be observed in certain peak values, at a value of 2942 cm^{-1}, some peaks are appearing corresponding to stretching vibrations of C–H, which explains the involvement of organic material or residuum in the sample composition, as reported elsewhere[20]. A peak at 1685 cm^{-1} has been correlated with C=O stretching vibrations, most probably from carbonyl groups or other organic residues. The peak at 1052 cm^{-1} corresponds to metal-oxygen (M–O) vibrations[21], thus confirming the ferrite structure. The peak at 431 cm^{-1} is assigned to the stretching vibrations of octahedral metal-oxygen in the spinel structure, a vital marker for the existence of the ferrite phase. There is an overall decrease in transmittance with decreasing wavenumber, demonstrating a trend that is characteristic of metal oxides due to the dominance of lower energy vibrations. The appearance of M–O bonds and the peaks of spinnel structure ensures structural integrity of the deposited film and the success in Mn-doping, which has promising use for catalytic and magnetic purposes. The vibrational properties may also affect the optical and electronic properties, which further makes this material suitable for supercapacitor and energy storage applications. Remnants of organic products formed in the synthesis process can be ascribed to the peaks existing at high wavenumber regions, which can be removed for better usability of the material in target applications. The FTIR analysis reveals major information on the vibrational modes of the Mn-doped Co-ferrite thin film, validating its structural characteristics and potential further functional applications.

UV-Vis spectra of Mn-doped Co-ferrite thin film

The UV-Vis spectra of the Mn-doped Co-ferrite thin film are depicted in Fig. 6. It was measured using a UV-1800 Series spectrophotometer at an absorbance mode for slit width 1.0 nm from 200 to 1200 nm. For

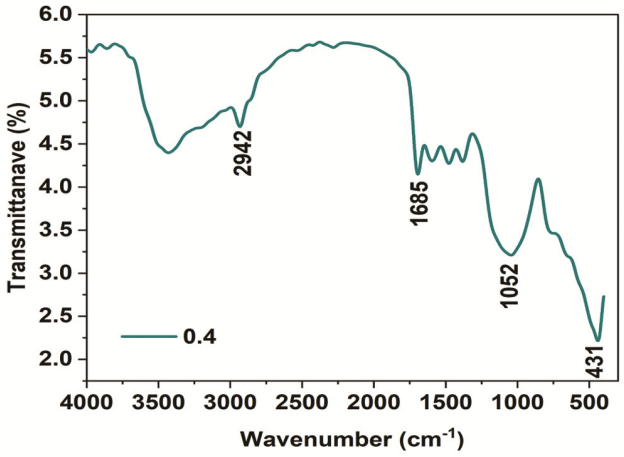

Fig. 5 — FTIR of Mn-doped Co-ferrite thin film x = 0.4

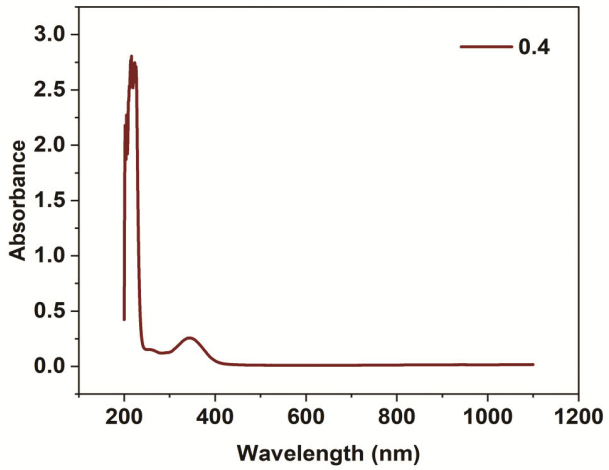

Fig. 6 — UV-Vis spectra of Mn-doped Co-ferrite thin film x = 0.4

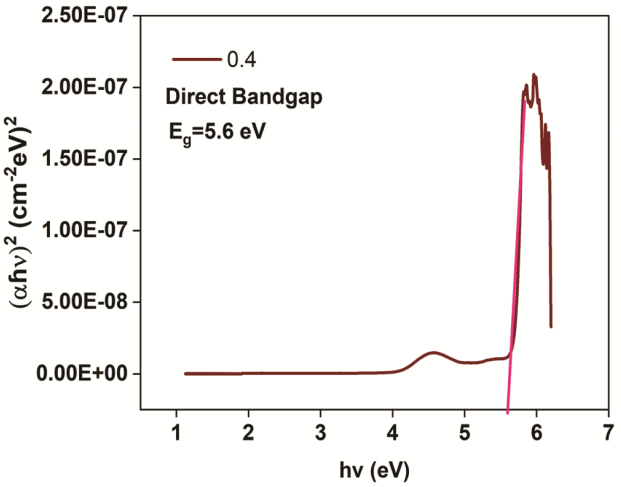

Fig. 7 — Touc's plot of Mn-doped Co-ferrite thin film x = 0.4

concentration at 1 mg in 100 mL, some clear peaks were observable of absorption related to the material due to electronic transition. For the sample with (x = 0.4), Abs = 3.25 at 215 nm and approximately at 347 nm, Abs = 0.77 was recorded. Strong electronic or band-to-band transitions are associated with this sample. Changes in the absorbance values and shifts in peak positions as a function of manganese content in Mn-doped Co-ferrite thin films may indicate the substitution of manganese that could change the electronic structure, and consequently the band gap might change[22]. Such changes might affect the d-d transitions and ligand field surrounding the metal ions; thus, these would impact the optical properties of the material. An understanding of such changes will help to optimize the optical property of the material for many applications, including sensors, catalysts, and electronics. Moreover, a cross-correlation between the UV-Vis spectra and the Raman spectra may advance the understanding of the structure, electronic, and vibrational properties of the material. This integrated analysis provides insights into potential applications of Mn doped Co ferrite thin films in areas where tailored optical and electronic properties are desired.

The given figure represents the Tauc plot of Mn-doped Co-ferrite thin film, specifically for the sample with (x = 0.4) as shown in Fig. 7. The vertical axis, $(\alpha h\nu)^2$, relates to the absorption coefficient and the energy of incident photons, while the horizontal axis displays the photon energy ($h\nu$) in electron volts (eV). The Kubelka-Munk function, F(R), is expressed by the equation[23];

$$F(R\infty) = \frac{(1-R\infty)^2}{2R\infty} \quad \ldots (1)$$

where ($R\infty$) is the diffuse reflectance, and α (the absorption coefficient) corresponds to the Tauc equation. From the plot, it can be observed that there is a direct bandgap (Eg) transition, with an extrapolated intercept on the x-axis indicating a bandgap energy of 5.6 eV. This suggests that the Mn-doped Co-ferrite thin film with (x=0.4) exhibits a wide direct bandgap, which is characteristic of semiconductor materials with potential applications in optoelectronic devices. The sharp increase in $(\alpha h\nu)^2$ at higher photon energies reflects the material's transition from low absorbance to a region of significant electronic absorption, signifying the onset of interband transitions[24]. The direct bandgap value of 5.6 eV positions this Mn-doped Co-ferrite thin film in the ultraviolet (UV) region of the electromagnetic spectrum, making it suitable for applications such as UV detectors, photocatalysis, or materials requiring wide bandgap semiconductors.

Raman spectra of Mn-doped Co-ferrite thin film

The Raman spectrum of the Mn-doped Co-ferrite thin film shows the predominant vibrational characteristics that reveal important structural and bonding details (Fig. 8). There are a number of sharp peaks that can be found along with the wavenumber range. Some of the strong peaks are at 1322 cm^{-1}, 3117 cm^{-1}, 3412 cm^{-1}, and 5728 cm^{-1}. Each one of the peaks is associated with different vibrational modes. These include lattice vibrations and metal-oxygen stretching inside the spinel structure[25]. This significant broad peak indicates complex interactions between cobalt, manganese, and iron ions and oxygen. Mn doping affects vibrational properties as seen through the shifts and broadening peaks, which are attributed to changes in bond lengths and the local structure caused by the substitution of Mn ions in ferrite lattices. The shift of the peaks to higher frequency might indicate strain in the crystal lattice, which could then be manifested in magnetic and electronic behavior. The broadening of some peaks may reflect less crystallinity or defects introduced by Mn doping. Therefore, Raman analysis shows manganese incorporation does indeed affect structural dynamics in Co-ferrite thin film, revealing a clue for its applicability in magnetic, electronic, and catalytic systems[26].

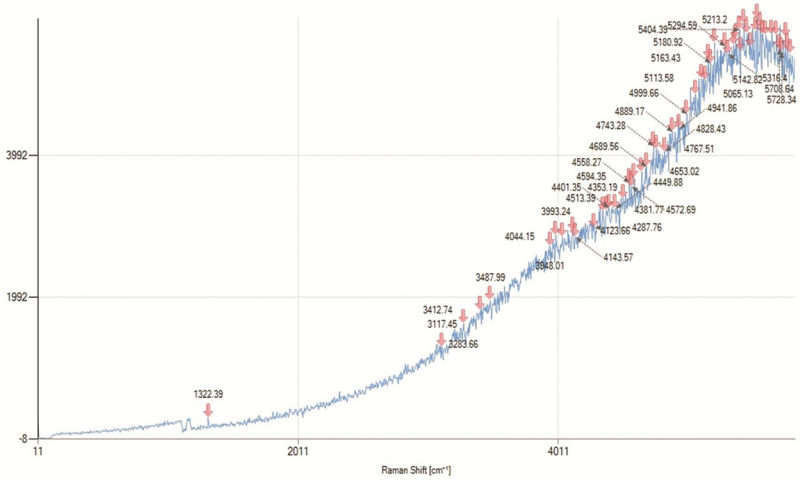

Fig. 8 — Raman Spectra of Mn-doped Co-ferrite thin film x = 0.4

Conclusions

The thin films of Mn-doped Co-ferrite show well-defined crystalline structure and XRD patterns show unique peaks at (111), (220), (311), (400), (511), (440), and (622) confirming single-phase cubic spinel formation. The films were deposited *via* spray pyrolysis. SEM and AFM analyses show a rough morphology with clustering, indicating agglomeration, due to surface energy effects. This agglomeration may make the films useful for applications like super capacitors. The inter-planar distance d values between 4.896 and 1.484 Å and the inter-ionic distances that decrease with the increase of Miller indices tend to crystalline behavior. FWHM values 0.338° - 0.497° indicate small crystal size, and the lattice constant of 8.418 Å was deduced from XRD data. FTIR spectra show that there is an important peak at 431 cm^{-1} characteristic of the stretching in the octahedral metal-oxygen in the spinel structure, which further supports the existence of the ferrite phase. Other peaks appearing in the range 1500-500 cm^{-1} are the bending vibrations of metal-oxygen, which further support the existence of the spinel structure. The obtained absorbance spectra by UV-Vis analysis indicated a major peak at 215 nm with an absorbance value of 3.25, and at around 347 nm, the value is found to be 0.77 for x = 0.4 sample; these peaks signify a maximum electronic transition. An approximate value of 5.6 eV is evaluated by Tauc's plots and found to have potential use for electronic and optical devices. From these results, Raman spectra provided additional information regarding the structural integrity and vibrational modes of the material, with peaks appearing at 1322 cm^{-1}, 3117 cm^{-1}, 3412 cm^{-1}, and 5728 cm^{-1}. Such peaks denote the influence of Mn doping on vibrational characteristics. The overlapping analysis of the structural, optical, and electronic properties of thin films of Mn-doped Co-ferrite makes it a promising material for technological application in supercapacitors, sensors, and energy storage devices.

Acknowledgement

The authors would like to extend their sincere gratitude to the Principal, Dayanand Science College, Latur, for their invaluable support and encouragement of this research. Their guidance and provision of resources have been instrumental in the successful completion of this work.

References

1 Rouhi M, Hajizadeh Z, Taheri-Ledari R, Maleki A & Babamoradi M, *Mat Sci Eng: B*, 286 (2022) 116021.
2 Gatzen H & Ruffert C, *ECS Transactions*, 3 (2007) 203.
3 Murakami N, Sakakibara K, (1989).
4 Jasrotia R, Prakash J, Saddeek Y.B, Alluhayb A.H, Younis A.M, Lakshmaiya N, Prakash C, Aly K, Sillanpää M & Ismail Y A, *Coord Chem Rev*, 522 (2025) 216198.
5 Ravina, Kumar S, Hashmi S, Srivastava G, Singh J, Quraishi A, Dalela S, Ahmed F & Alvi P, *J Mat Sci: Mat Elec*, 34 (2023) 868.
6 Dash J, Aiyar R, Prasad S, Venkataramani N, Date S, Kulkarni S, Kishan P & Kumar N, *J Mag Mag Mat*, 226 (2001) 1636.
7 Rathod V, Anupama A, Jali V, Hiremath V & Sahoo B, *Ceramics Int*, 43 (2017) 14431.
8 Mahmoudi M & Kavanlouei M, *Int J Mat Res*, 105 (2014) 1097.
9 Chaudhari M N, Ahirrao R B & Bagul S D, *Int J Res Appl Sci Eng Tech*, 9 (2021) 5215.

10 Kate R S, Pathan H M, Kalubarme R, Kale B B & Deokate R J, *J Energy Storage*, 54 (2022) 105387.
11 Ismael M, Sharma A & Kumar N, *Sust Mat Tech*, (2024) e00826.
12 Workie A.B, Ningsih H.S & Shih S-J, *J Anal App Pyrol*, 170 (2023) 105915.
13 Santos-Gómez L D, Zamudio-García J, Porras-Vázquez J.M, Losilla E R & Marrero-López D, *J Power Sources*, 507 (2021) 230277.
14 Roy I, *Rensselaer Polytechnic Institute*, 2020.
15 Khavale S, Ambare R & Lokhande B, *J Mat Sci Mat Elect*, 31 (2020) 7315.
16 Rossi Z, Ghannam H, Brioual B, Ullah S, Zanouni M, Diani M, Aouni A & Addou M, *Crystal Res Tech*, 59 (2024) 2300235.
17 Murugesan C, Ugendar K, Okrasa L, Shen J & Chandrasekaran G, *Ceramics Int*, 47 (2021) 1672.
18 Katkar P K, Marje S J, Parale V G, Lokhande C D, Gunjakar J L, Park H-H & Patil U M, *Langmuir*, 37 (2021) 5260.
19 Hassan E S, Qader K Y, Hadi E H, Chiad S S, Habubi N F, Abass K H, *Nano Biomed Eng*, 12 (2020) 205-213.
20 Demircan G, Yalcin S, Alivi K, Ceyhan G, Acikgoz A, Balak M V, Aktas B & Das R, *Optical Mat*, 126 (2022) 112163.
21 Jirátová K, Perekrestov R, Dvořáková M, Balabánová J, Koštejn M, Veselý M, Čada M, Topka P, Pokorná D, Hubička Z, *Catalysts*, 11 (2021) 1453.
22 Tian J.-l, Yan H.-T, Hu Q, Liu R.-X, Liu L.-M & Liu Y.-C, *J Mol Struc*, 1289 (2023) 135842.
23 Landi S, Segundo I.R, Freitas E, Vasilevskiy M, Carneiro J & Tavares C J, *Solid State Comm*, 341 (2022) 114573.
24 Ansari S, Phase D, Kolekar Y & Ramana C, *Mat Sci Eng B*, 300 (2024) 117134.
25 Shi M, Chen H, Du S, Xu Y, Zuo R, Bai T & Men E, *J Mat Sci: Mat Elect*, 34 (2023) 1635.
26 Wang H, Liu L, Zhao J, Qin B, Zhang Y & Yang W, *Mat Res Bull*, 173 (2024) 112684.